Journal of Magnetism and Magnetic Materials 623 (2025) 173013

Contents lists available at ScienceDirect

Journal of Magnetism and Magnetic Materials

journal homepage: www.elsevier.com/locate/jmmm

Research article

Testing of magnetic properties of amorphous and nanocrystalline alloys applied out-of-plane stress at wide frequency range

Changgeng Zhang *, Guochen Niu, Wenbin Meng, Yongjian Li

Hebei University of Technology, 300401 Tianjin, China

ARTICLE INFO

Keywords:
Out-of-plane stress
Amorphous alloy
Nanocrystalline alloy
Magnetic properties

ABSTRACT

Nanocrystalline and amorphous alloys are extensively utilized as core materials in devices such as motors and transformers. Their magnetic properties can be altered by stress, significantly impacting the operational efficiency and reliability of electrical equipment. In this study, a wide-frequency-range magnetic property testing system capable of applying out-of-plane stress is designed. The design of the stress application components and the uniformity of stress distribution in the samples are thoroughly analyzed through simulations. This system is used to measure the changes in the magnetic properties of nanocrystalline and amorphous alloy sheets under out-of-plane stress over a wide frequency range. The test results indicate that the out-of-plane stress applied to nanocrystalline alloys leads to an increase in the core loss. The core loss in amorphous alloys initially decreases and subsequently increases at frequencies exceeding the kilohertz range.

1. Introduction

Nanocrystalline and amorphous alloys are widely used in the cores of motors and high-frequency transformers due to their excellent soft magnetic properties, such as low coercivity, low loss, and high permeability [1–4]. During the stacking and cutting processes involved in manufacturing motor stator cores, internal stress is inevitably introduced into the alloys. In industrial practice, annealing is used to eliminate stress [5]. However, motor cores are also exposed to complex external stresses during assembly and operation, including those from fixed structures [6], self-weight, and pressure exerted by seawater on deep-sea motors [7]. Similarly, the nanocrystalline and amorphous alloy cores used in high-frequency transformers are subjected to external stresses from the winding process, clamps, and bolts [8]. These factors cause nanocrystalline and amorphous alloys to operate under mechanical stress. The magnetic properties of these alloys are highly sensitive to stress [9,10], which affects the performance of the equipment during operation and, especially in severe conditions, leads to overheating and damage. If the impact of stress is not considered in the core design, an accurate analysis of the existing equipment becomes impossible. Therefore, it is essential to study the magnetic properties of nanocrystalline and amorphous alloys under stress conditions.

The effects of different stresses on the magnetic properties of electrical steel sheets have been studied. Vertical rotating single-sheet testers have been widely used to study how in-plane stress affects the magnetic properties of electrical steel sheets [11–13]. The testing devices were designed to apply out-of-plane stress (normal stress perpendicular to the plane) to strip and ring-shaped samples [14–16]. Nevertheless, the uniformity of the out-of-plane stress applied by these devices requires further refinement. Although considerable research has been devoted to nanocrystalline and amorphous alloys, limited studies have focused on their magnetic properties under stress. In-plane tensile and compressive stresses were applied along the magnetization direction to single-layer and stacked amorphous alloy sheets, and the effects of stress under low-frequency conditions on their magnetic properties were investigated [17]. Subsequently, the testing frequency was extended to 4 kHz [10]. The impact of stress on the magnetic properties of amorphous alloy cores has been examined [8,18]. Currently, research on the magnetic properties of nanocrystalline and amorphous alloys under stress has primarily focused on the effects of in-plane stress. However, research on the effects of out-of-plane stress on magnetic properties remains scarce. Moreover, previous studies on the magnetic properties of amorphous alloys, primarily focusing on low frequencies, are insufficient for the design of high-frequency transformers.

In this study, a new single-sheet tester (SST) that can apply uniform out-of-plane stress (hereafter refers to as normal stress) is designed. Through using a nanocrystalline yoke and insulating the entire device, it can test samples in the range of 50 Hz to 15 kHz. For the first time, the

* Corresponding author.
E-mail address: changgeng.zhang@hebut.edu.cn (C. Zhang).

https://doi.org/10.1016/j.jmmm.2025.173013
Received 21 January 2025; Received in revised form 18 March 2025; Accepted 26 March 2025
Available online 31 March 2025
0304-8853/© 2025 Elsevier B.V. All rights are reserved, including those for text and data mining, AI training, and similar technologies.

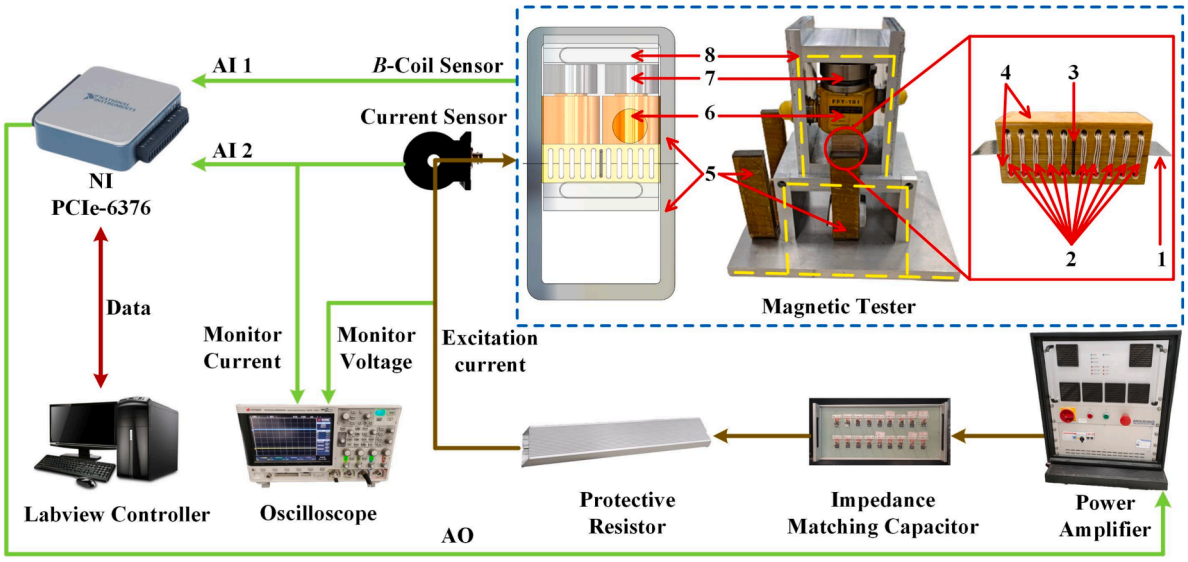


Fig. 1. Magnetic property testing system. 1-sample placement, 2-excitation windings, 3-*B*-coil sensor, 4-fixture, 5-yoke, 6-component providing stress in the laminate direction, 7-stress sensor, and 8-support frame.

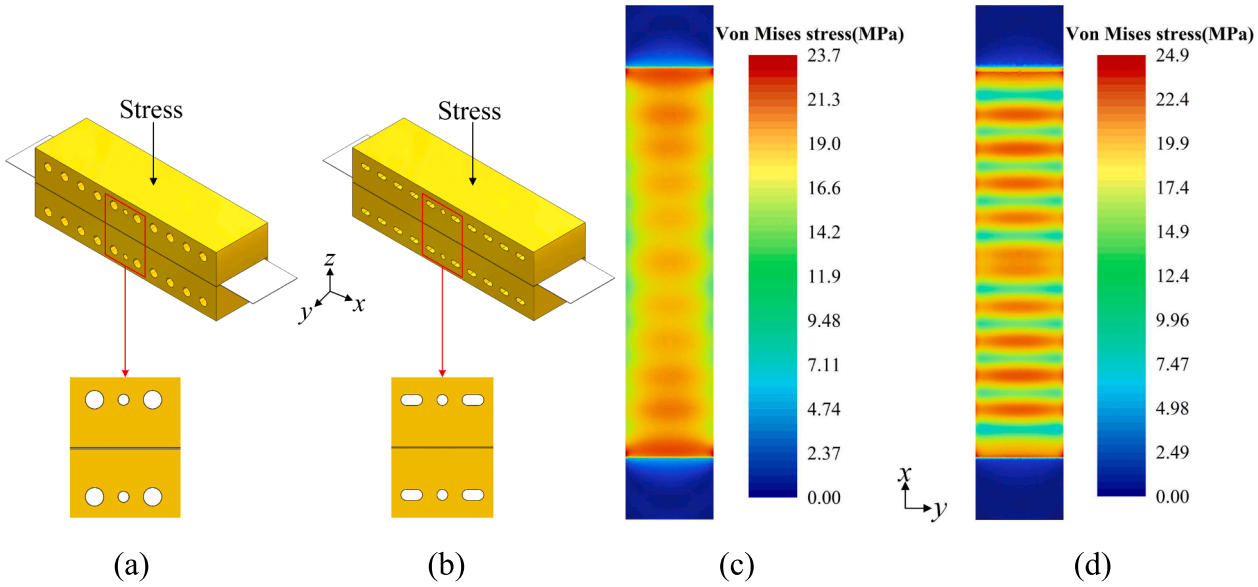


Fig. 2. (a) Circular through-holes (b) Straight slot through-holes (c) Circular through-holes stress distribution (d) Straight slot through-holes stress distribution.

Table 1
Material Properties of the Sample and Clamp.

Parameters	Epoxy Resin	Nanocrystalline	Amorphous
Young's Modulus [GPa]	2	150	110
Poisson's Ratio	0.35	0.30	0.30
Density [kg/m^3]	2360	7300	7180

Table 2
Relative standard deviations corresponding to different through-hole positions.

The distance of the through-holes from the sample	Relative Standard Deviation
12 mm	1.35×10^{-1}
14 mm	9.71×10^{-2}
16 mm	8.93×10^{-2}

magnetic properties of an 18 μm thick single nanocrystalline alloy sheet and a 25 μm thick single amorphous alloy sheet, which have been subjected to ordinary vacuum annealing, are measured under different normal stresses, and the impact of normal stress on the magnetic properties of the samples is analyzed.

2. Design of measurement system

The overall schematic of the test system is presented in Fig. 1, which includes a LabVIEW controller, data acquisition card, power amplifier, current sensor, oscilloscope, protective resistor, impedance matching capacitor, and magnetic tester. The LabVIEW controller with a data acquisition card generates a sinusoidal voltage signal, which is amplified by a power amplifier and applied to the exciting windings, creating a sinusoidal AC magnetic field in the sample. The current and voltage signals from the current sensor and *B*-coil sensor are collected by the data acquisition card. These signals are then processed by the LabVIEW

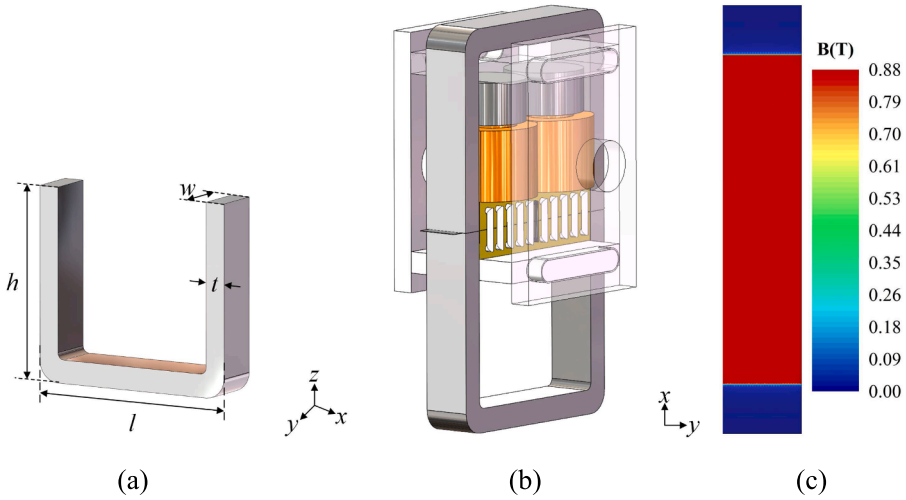


Fig. 3. (a) Dimensions of the yoke (b) Simulation model (c) *B* distribution in the sample.

Table 3
Sample parameters and dimensions.

Name	Chemical Composition	Length (mm)	Width (mm)	Thickness (μm)
Nanocrystalline (1K107B)	FeCuNbSiB	168	30	18
Amorphous (1 K101)	FeSiB	168	30	25

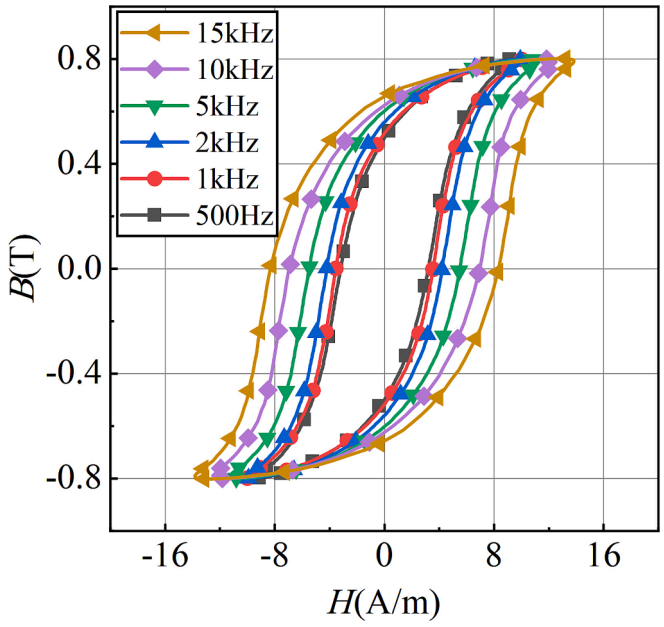


Fig. 4. Magnetic properties of nanocrystalline alloys at wide frequency range.

controller to obtain the *B*, *H*, and loss values. The frequency-domain feedback control algorithm and waveform compensation method of the LabVIEW system ensure that the *B* waveform remains sinusoidal [19]. During the experiment, the oscilloscope monitors the output voltage of the power amplifier and the current in the exciting windings to prevent the power amplifier's output voltage and current from exceeding their limits and the windings' capacity. The value of normal stress can be directly read by the stress sensors. The data acquisition card used in this study is the National Instruments PCIe-6376, which has a sampling rate of 3.5 MS/s and supports signal acquisition at frequencies of up to 15 kHz.

The stress-loading system consists of a clamp, components for applying normal stress, a stress sensor, and a supporting frame. The sample is positioned between two insulating blocks that constitute the clamp. These insulating blocks are fabricated from smooth-surfaced epoxy resin, which has excellent insulating properties (relative permeability ≈1, insulation resistance $> 10^{12}$ Ω) and high compressive strength (flexural strength > 340 MPa). Eleven through-holes are evenly distributed on the side of each insulation block. The excitation windings and *B*-coil sensor are wound through these holes, allowing normal stress to be directly applied to the clamp and subsequently transferred to the sample. The components responsible for applying normal stress utilize a hydraulic mechanism to exert stress on the clamp. Each side of the supporting frame includes a through-hole that allows the oil supply hoses from the hydraulic device to pass through. This device can exert a force of 7.2×10^4N (20 MPa). The force is measured using a stress sensor with an overall accuracy of ± 0.1 %FS.

2.1. Structural mechanical analysis

To validate the experimental results, it is essential to ensure a uniform distribution of stress within the sample. This can be assessed by analyzing the mechanical design of the clamp. To determine the specific design parameters of the clamp, extensive simulation studies were conducted, including the effects of different through-hole shapes and heights of the through-holes relative to the sample. Fig. 2 shows the design and simulation results for straight slot through-holes and circular through-holes in the clamp. To maintain consistency for comparison, the areas of the straight and circular slots were kept the same. During the simulation, a vertical force of 7.2×10^4N was applied to the clamp, and the stress distribution was depicted using the Von Mises stress distribution. The material properties of the samples and clamps are presented in Table 1.

As shown in Fig. 2(c) and 2(d), the maximum Von Mises stress in the sample under the clamp with circular through-holes is reduced compared to that under the clamp with straight slot through-holes. Additionally, the simulation results indicate that the stress distribution with circular through-holes is more uniform, with a relative standard deviation of 9.71×10^{-2}, compared to a relative standard deviation of 1.61×10^{-1} for straight slot through-holes. This represents a 40 % reduction in the relative standard deviation. The relative standard deviation (RSE) is calculated using the following formula,

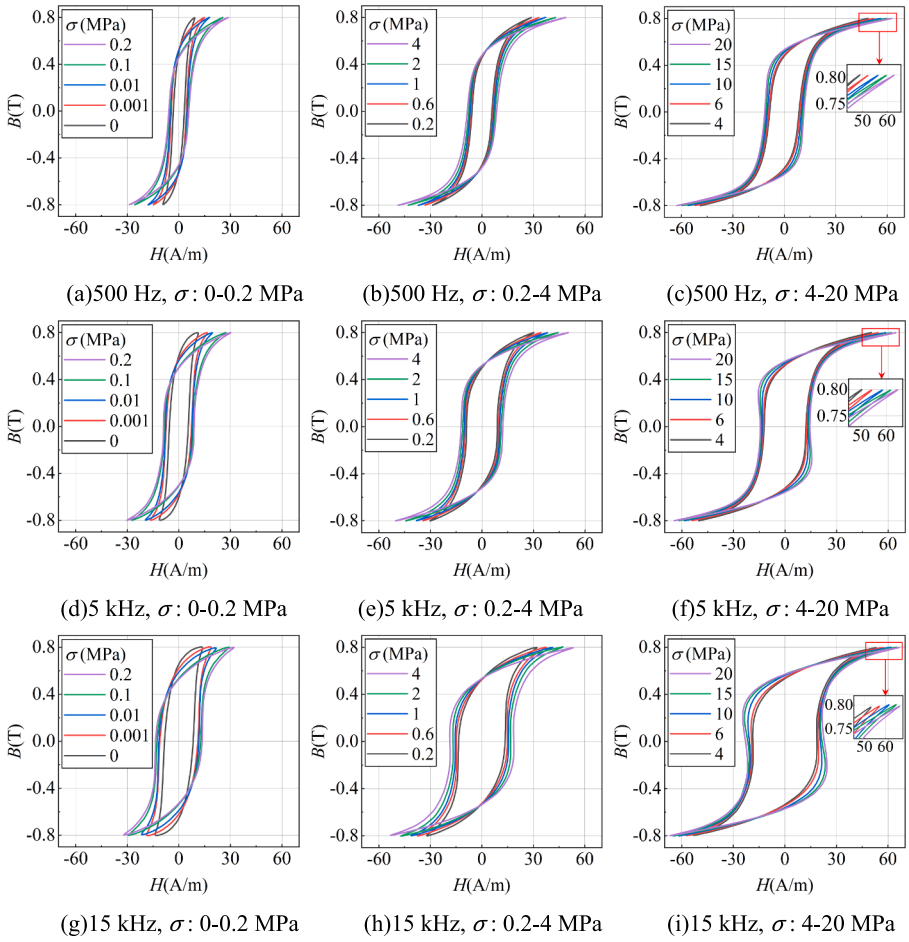


Fig. 5. Hysteresis loops under normal stress at 0.8 T.

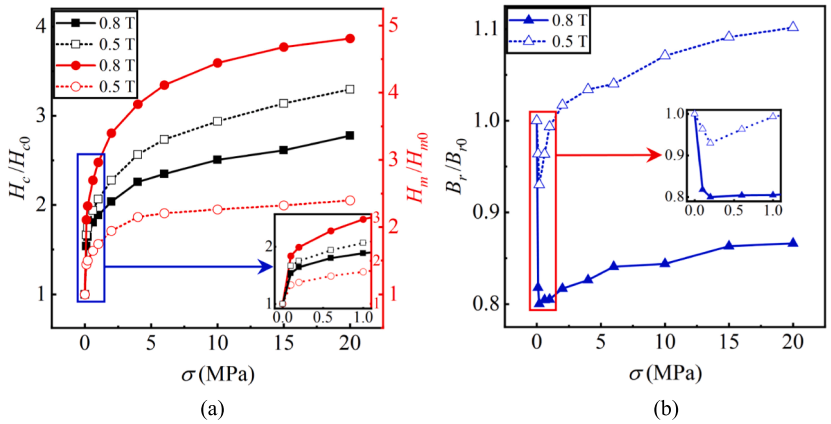


Fig. 6. Relative change in (a) magnetic field strength, H_m, coercive field, H_c, and (b) remanence, B_r, at 15 kHz.

$$\mathrm{RSE} = \frac{\sigma}{\mu} \tag{1}$$

where σ is the standard deviation of the Von Mises stress in the sample and μ is the mean of the Von Mises stress in the sample.

Another design enhancement involves the optimization of the through-hole height relative to the sample. The relative standard deviations of the stress distributions at varying heights are listed in Table 2. As the height of the through-holes relative to the sample increases, the stress uniformity improves. Specifically, increasing the height to 14 mm resulted in a 30 % enhancement in uniformity compared to 12 mm. However, increasing the height to 16 mm results in only a 10 % marginal improvement over the 14 mm height. Additionally, the clamp's reliability must be considered, as positioning the through-holes too close to the clamp's outer edge may cause damage. Considering these factors, a height of 14 mm from the sample to the center of the through-holes was selected.

2.2. Electromagnetic analysis

In addition to mechanical stress analysis for optimizing fixture shape,

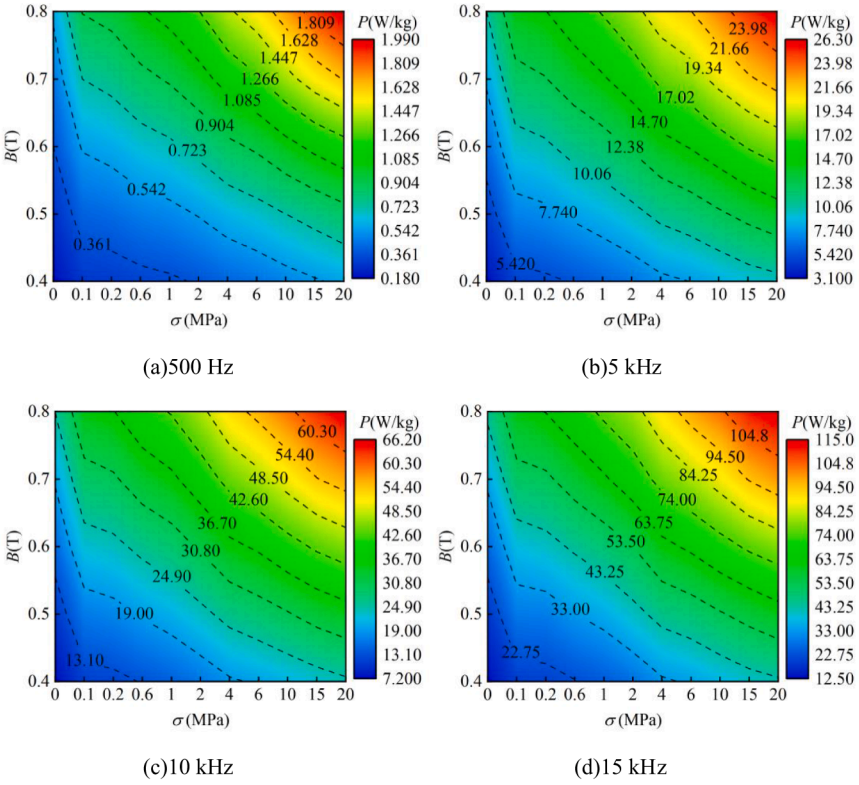


Fig. 7. Effect of normal stress on core loss of nanocrystalline alloy.

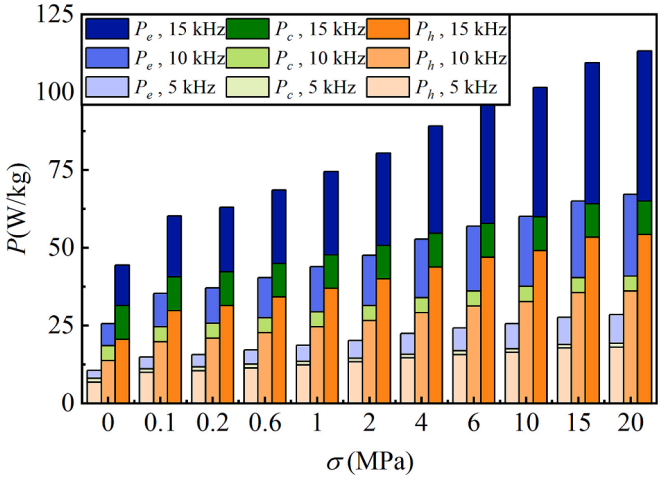


Fig. 8. Hysteresis, eddy current and excess loss components under different frequencies and normal stress at 0.8 T.

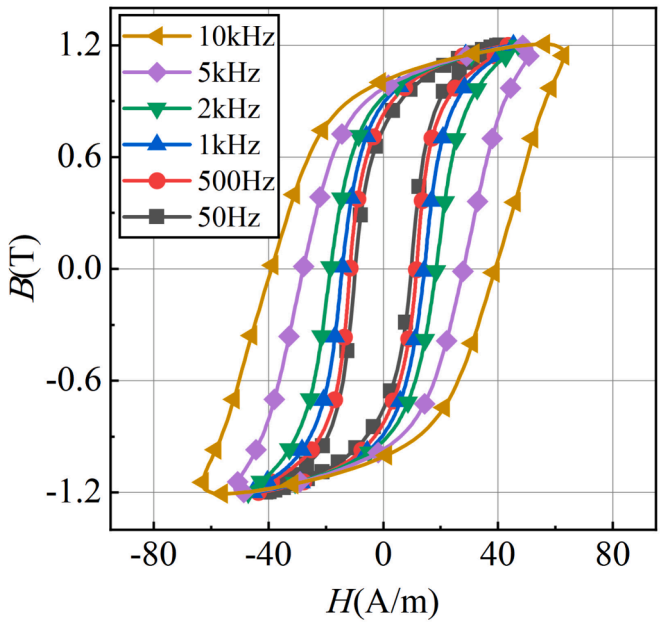


Fig. 9. Magnetic properties of amorphous alloys at wide frequency range.

electromagnetic simulations are essential for understanding the electromagnetic field distribution within the sample. A three-dimensional electromagnetic finite element analysis (FEA) was conducted to address this issue. The device parameters prior to FEA are provided below. As shown in Fig. 3(a) and 3(b), a double U-shaped yoke made of nanocrystalline alloy(1K107B) was selected to establish a closed magnetic circuit for the magnetic flux during testing. The yoke measures 154 mm in length(l), 35 mm in width(w), 142 mm in height(h), and 15 mm in thickness(t). The excitation winding is made using Litz wire with a diameter of 1 mm, wound through 10 through-holes with 3 turns per hole, totaling 30 turns. The B-coil was wound with 10 turns in the smaller through-hole located in the center. The dimensions and chemical compositions of the samples are provided in Table 3. When a current of 0.2 A is applied to the excitation winding, the simulation results of the magnetic flux density(B) distribution within the sample are shown in Fig. 3(c). The results indicate that the magnetic flux within the sample is uniformly distributed between the inner walls of the yoke, with an average flux density of approximately 0.8 T.

The device's support frame is constructed from aluminum alloy, which possesses excellent electrical conductivity comparable to that of the nanocrystalline yoke. During tests conducted at frequencies

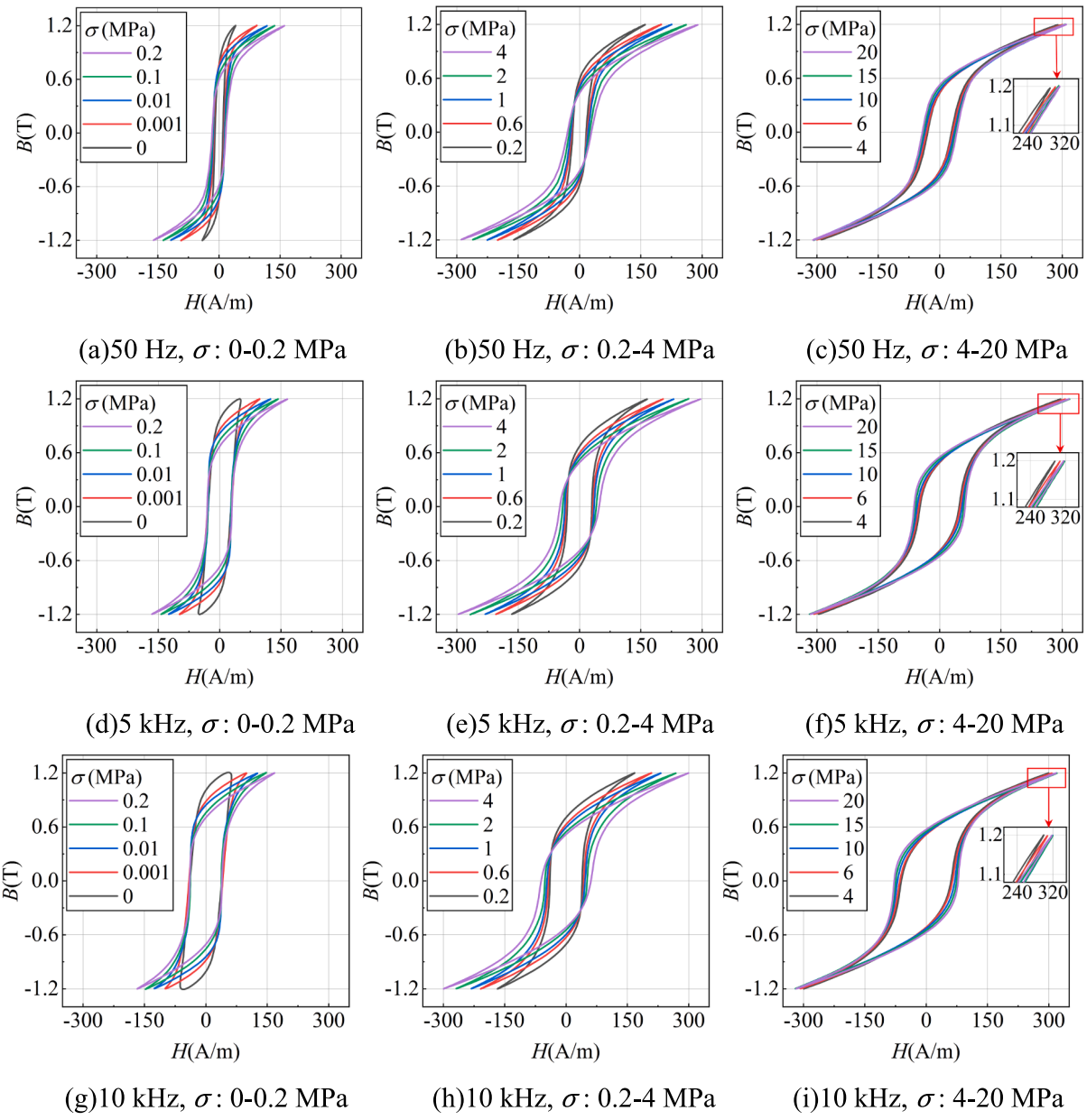


Fig. 10. Hysteresis loops under normal stress at 1.2 T.

exceeding the kilohertz range, leakage flux can induce eddy currents within the aluminum alloy frame. Direct contact between the support frame and yoke allows these eddy currents to be induced inside the magnetic core and sample, leading to inaccuracies in the test results. Therefore, an insulation layer is applied to the external surfaces of both the frame and the yoke to mitigate this effect and ensure accurate results exceeding the kilohertz range.

3. Results and discussion

The frequency range investigated in this study, from 50 Hz to 15 kHz, comprehensively encompasses all operational frequencies for amorphous and nanocrystalline alloys used as high-frequency transformers or motor cores [20–23]. The normal mechanical stress typically encountered by motor or transformer cores is generally below 20 MPa [24–26]. Furthermore, due to the sensitivity of nanocrystalline and amorphous alloys to low stress, the applied normal stress range in this study was from 0 to 20 MPa, with the step size of the normal stress gradually increasing. All experiments in this study are carried out at room temperature (25 °C).

3.1. Nanocrystalline

The alternating magnetic properties of nanocrystalline alloy (1K107B) are measured under various normal stress conditions and varying frequencies. Fig. 4 depicts the hysteresis loops of the nanocrystalline alloy at a constant maximum B of 0.8 T, across frequencies ranging from 500 Hz to 15 kHz. As the frequency increases, the eddy currents within the nanocrystalline alloy progressively intensify, resulting in the broadening of the hysteresis loops.

Fig. 5 illustrates the hysteresis loops of the nanocrystalline alloy at various frequencies under normal stress. It is observed that as the normal stress increases, both the coercivity (H_c) and the maximum magnetic field intensity (H_m) of the nanocrystalline alloy increase. An increase in H_m also signifies a gradual reduction in magnetic permeability. This indicates that the application of normal stress to the sample has altered

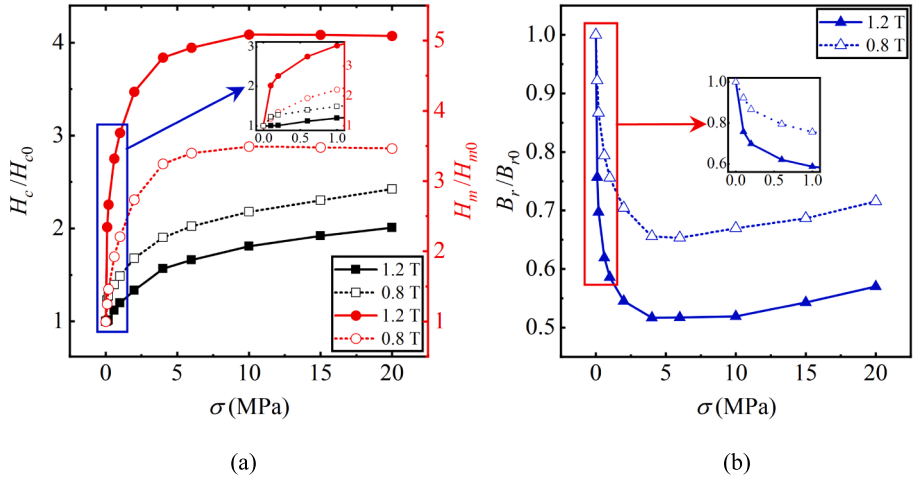


Fig. 11. Relative change in (a) magnetic field strength, H_m, coercive field, H_c, and (b) remanence, B_r, at 10 kHz.

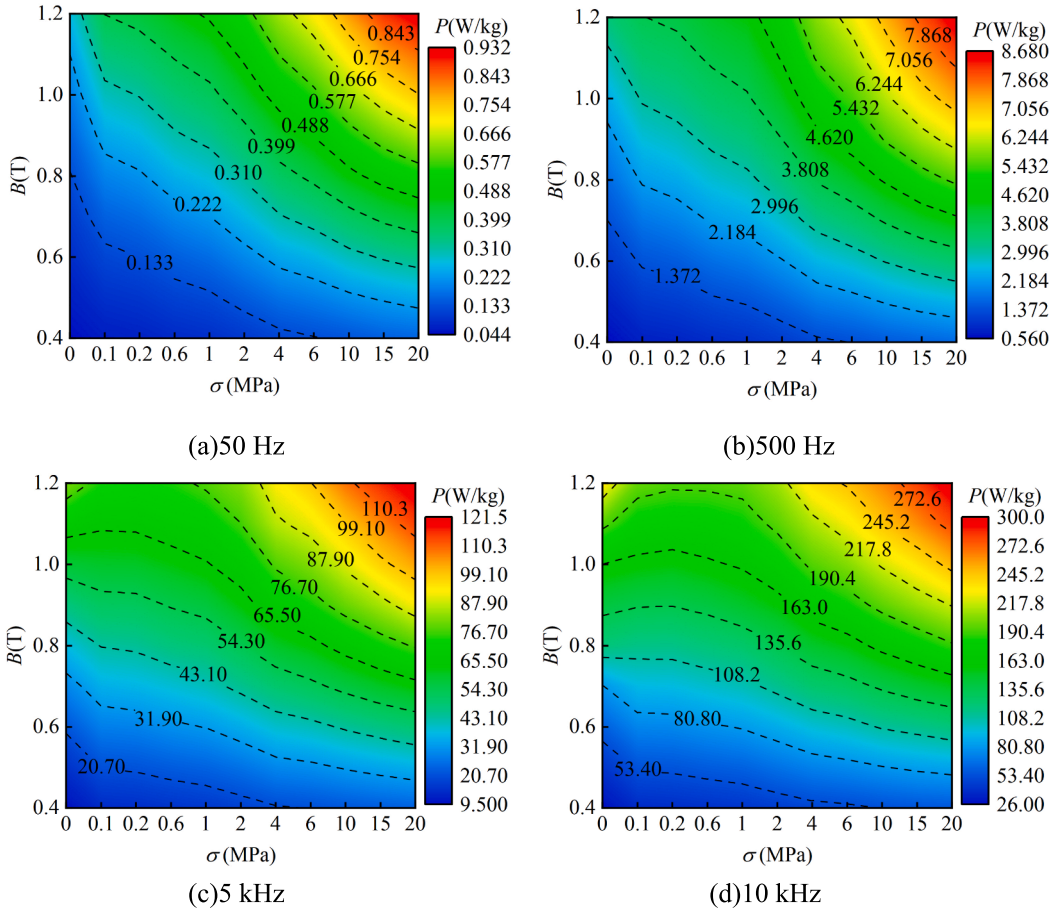


Fig. 12. Effect of normal stress on core loss of amorphous alloy.

its magnetic anisotropy [27]. From Fig. 5(c), 5(f), and 5(i), it is observed that when the stress exceeds 4 MPa, the hysteresis loops gradually deform into an S-shape with increasing stress, a trend that becomes more pronounced at higher frequencies. Furthermore, the hysteresis loops at different stress levels intersect at two points that are symmetrical with respect to the origin.

Fig. 6(a) and 6(b) illustrate the relative changes in the coercivity (H_c), maximum magnetic field intensity (H_m), and remanence (B_r) of the nanocrystalline alloy under stress at a frequency of 15 k Hz. Here, H_{m0}, H_{c0}, and B_{r0} represent the corresponding parameters in the unstressed state. Compared to high magnetic flux density, the change in coercivity is more pronounced at low magnetic flux densities, whereas the opposite is true for the maximum magnetic field intensity. Relative to the maximum magnetic field intensity at 0 MPa, a normal stress of 20 MPa can increase the maximum magnetic field intensity by nearly 2.5-fold at 0.5 T and by 5-fold at 0.8 T. The change in remanence with increasing normal stress is non-monotonic; it decreases under normal stress below 0.2 MPa and increases beyond this stress level. At 0.8 T, the remanence

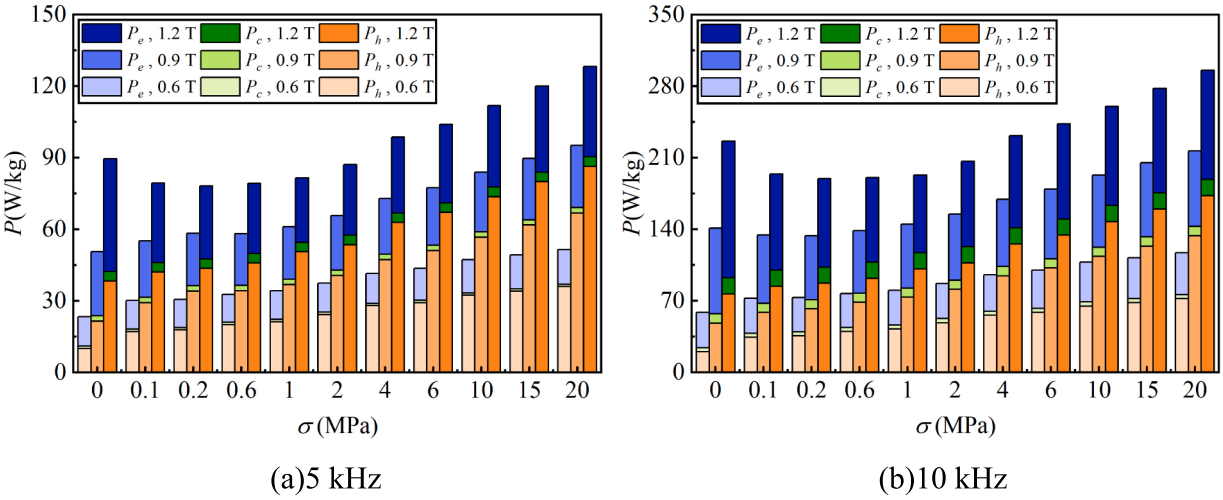


Fig. 13. Hysteresis, eddy current and excess loss components under normal stress at different frequencies and magnetic flux densities.

does not exceed the zero-stress value, whereas at 0.5 T, it surpasses the zero-stress value. Additionally, the impact of normal stress on remanence is markedly less than its effect on coercivity and maximum magnetic field intensity, a trend consistent with observations in other isotropic soft magnetic materials [10]. When the stress surpasses 4 MPa, the relative changes in all parameters exhibit a linear correlation with the increase in stress.

Fig. 7 presents the core loss of the nanocrystalline alloy under normal stress at magnetic flux densities ranging from 0.4 T to 0.8 T and frequencies of 500 Hz, 5 kHz, 10 kHz, and 15 kHz. As the normal stress increases, the core loss also increases, but the rate of increase gradually slows down. This indicates a nonlinear relationship between core loss increase and normal stress. Comparing the core loss results at different magnetic flux densities, under a condition of 20 MPa at 5 kHz and 0.4 T, the core loss increased by 202.16 % compared to the 0 MPa condition. Under the same conditions, at 0.8 T, the core loss increased by 161.55 %. This demonstrates that the core loss of the nanocrystalline alloy is more sensitive to normal stress at lower magnetic flux densities than at higher ones. As the frequency increases, the growth rate of core loss at 0.8 T under 20 MPa decreases from 192.94 % at 500 Hz to 153.65 % at 15 kHz.

Under sinusoidal magnetic flux conditions, the formula for core loss based on Bertotti's loss separation theory is as follows [28]:

$$P = P_h + P_c + P_e = k_h B_m^2 f + \frac{\pi^2 d^2}{6\rho\sigma} B^2 f^2 + k_e B_m^{1.5} f^{1.5} \tag{2}$$

where P_h is the hysteresis loss, P_c is the eddy current loss, and P_e is the excess loss. Coefficients k_h and k_e represent the hysteresis and excess loss coefficients, respectively. B_m and f denote the peak magnetic flux density and frequency, respectively. Additionally, d,ρ, and σ represent the thickness, density, and electrical resistivity of the material, respectively.

As shown in Fig. 8, the eddy current loss constitutes a relatively small portion of the total loss and remains nearly unaffected by stress under constant frequency and magnetic flux density. At 5 kHz, hysteresis loss is the predominant component of core loss, and the impact of normal stress on the core loss is primarily attributed to hysteresis loss. As the frequency rises, the proportion of excess loss gradually increases, resulting in variations in the core loss determined by both hysteresis and excess loss.

3.2. Amorphous

The alternating magnetic properties of amorphous alloy (1 K101) are measured under various normal stress conditions and at different frequencies. Fig. 9 illustrates the hysteresis loops of the amorphous alloy at a constant maximum B of 1.2 T, across frequencies ranging from 50 Hz to 10 kHz. As the frequency increases, the changes in the hysteresis loops of the amorphous alloy are similar to those observed in the nanocrystalline alloy. However, at 10 kHz, the area of the hysteresis loop for the amorphous alloy exhibits a more substantial increase compared to the nanocrystalline alloy, indicating higher losses in the amorphous alloy at elevated frequencies.

Fig. 10 shows the hysteresis loops of the amorphous alloy under different frequencies and normal stresses. As the normal stress increases, the hysteresis loops of the amorphous alloy exhibit a greater degree of inclination than those of the nanocrystalline alloy. Furthermore, the hysteresis loops under different stress levels intersect at two points that are symmetric with respect to their origin.

Fig. 11(a) and 11(b) show the relative changes in the coercivity (H_c), maximum magnetic field strength (H_m), and remanence (B_r) of the amorphous alloy under stress at a frequency of 10 kHz. Here, H_{c0}, H_{m0}, and B_{r0} represent the corresponding parameters in the unstressed state. As the normal stress increases, the changes in these parameters for the amorphous alloy are similar to those observed in the nanocrystalline alloy. However, once the stress exceeds 10 MPa, the maximum magnetic field strength of the amorphous alloy approaches saturation. The remanence of the amorphous alloy initially decreases and then increases with increasing normal stress, with the turning point occurring at approximately 5 MPa. The increase in remanence does not exceed the zero-stress value. When the stress exceeds 6 MPa, the relative changes in coercivity and remanence exhibit a linear relationship with increasing stress.

Fig. 12 presents the core losses of the amorphous alloy under normal stress at magnetic flux densities ranging from 0.4 T to 1.2 T, at frequencies of 50 Hz, 500 Hz, 5 kHz, and 10 kHz. At 50 Hz and 500 Hz, the core losses gradually increase with increasing normal stress. At 5 kHz and 10 kHz, the core losses initially decrease and then increase with increasing normal stress at higher magnetic flux densities. However, at 20 MPa, core losses continue to increase, consistent with findings observed in non-oriented silicon steel [14,26]. Furthermore, as frequency increases, the magnetic flux density threshold for loss reduction gradually shifts to lower values.

Fig. 13 illustrates that as normal stress increases, the eddy current loss remains almost constant, while the hysteresis loss continuously increases, and the excess loss does not change monotonically. At low magnetic flux densities, the variation in the excess loss with normal stress is minimal, and changes in the core loss are primarily dominated by the hysteresis loss. At high magnetic flux densities, the excess loss initially decreases and then increases with increasing normal stress. At

low frequencies, the proportion of excess loss is small; as the normal stress increases, the decrease in excess loss is less than the increase in hysteresis loss. Therefore, at 50 Hz and 500 Hz, the core loss increases with increasing stress. At high frequencies, the excess loss increases because of the higher frequency. With increasing normal stress, the decrease in the excess loss is greater than the increase in the hysteresis loss, resulting in a decrease in the core loss.

4. Conclusion

This study presents a broadband magnetic property testing apparatus designed to measure the magnetic performance of nanocrystalline and amorphous alloys under normal stress. To achieve a uniform stress distribution on the samples, an optimal through-holes design is selected to apply a maximum normal stress of 20 MPa. The magnetic properties of nanocrystalline alloy (1K107B) and amorphous alloy (1K101) are measured and analyzed under normal stress within the frequency range of 50 Hz to 15 kHz. The results demonstrate that the samples' magnetic properties are strongly dependent on normal stress, and the application of stress modifies their magnetic anisotropy. This study provides valuable insights for modeling and calculating the magnetic properties of nanocrystalline and amorphous alloys used in motors and high-frequency transformers under operational conditions.

CRediT authorship contribution statement

Changgeng Zhang: Writing – review & editing, Supervision, Funding acquisition. **Guochen Niu:** Writing – review & editing, Writing – original draft, Methodology, Data curation. **Wenbin Meng:** Validation, Software. **Yongjian Li:** Writing – review & editing, Supervision, Funding acquisition.

Declaration of competing interest

The authors declare that they have no known competing financial interests or personal relationships that could have appeared to influence the work reported in this paper.

Acknowledgments

This work was supported in part by the National Natural Science Foundation of China, (Nos. 52277008, 52130710), and Natural Sciences foundation of Hebei Province, China (E2023202050).

Data availability

The authors do not have permission to share data.

References

[1] Z. Wang, R. Masaki, S. Morinaga, et al., Development of an axial gap motor with amorphous metal cores, IEEE Trans. Ind. Appl. 47 (3) (2011) 1293–1299.
[2] S. Okamoto, N. Denis, Y. Kato, et al., Core loss reduction of an interior permanent-magnet synchronous motor using amorphous stator core, IEEE Trans. Ind. Appl. 52 (3) (2016) 2261–2268.
[3] A. Yao, T. Sugimoto, S. Odawara, et al., Core loss properties of a motor with nanocrystalline rotor and stator cores under inverter excitation, IEEE Trans. Magn. 54 (11) (2018) 1–5.
[4] Y. Guo, L. Liu, W. Yin, et al., Developing high-power-density electromagnetic devices with nanocrystalline and amorphous magnetic materials, Nanomaterials 13 (13) (2023) 1963.
[5] N. Nishiyama, K. Tanimoto, A. Makino, Outstanding efficiency in energy conversion for electric motors constructed by nanocrystalline soft magnetic alloy "NANOMET®" cores. AIP Advances, 2016, 6(5).
[6] D. Miyagi, Y. Aoki, M. Nakano, et al., Effect of compressive stress in thickness direction on iron losses of non-oriented electrical steel sheet, IEEE Trans. Magn. 46 (6) (2010) 2040–2043.
[7] J. Zou, W. Qi, Y. Xu, et al., Design of deep sea oil-filled brushless DC motors considering the high pressure effect, IEEE Trans. Magn. 48 (11) (2012) 4220–4223.
[8] L.H. Zhu, Y.H. Shi, Q.X. Yang, Effect of clamping force on magnetic properties and core vibration of amorphous alloys, Proc. CSEE 40 (24) (2020), pp. 8155–8164+8252.
[9] C. Swieboda, D. Grybos, J. Leszczynski, et al. Influence of normal-compressed stresses on measurement precision of toroidal and oval nanocrystalline cut cores used for metering, in: 2018 Innovative Materials and Technologies in Electrical Engineering (i-MITEL). IEEE, 2018: 1-4.
[10] X. Zhu, Y. Li, Y. Dou, et al., Effect of uniaxial stress on magnetic property of laminated amorphous sheets up to kilohertz range, AIP Adv. 14 (1) (2024) 015150.
[11] P. Rękas, M. Nowicki, P. Gazda, et al., A measuring setup for testing the mechanical stress dependence of magnetic properties of electrical steels, J. Magn. Magn. Mater. 577 (2023) 170791.
[12] Y. Dou, Y. Li, C. Zhang, et al., Effects of uniaxial stress along different directions on alternating magnetic properties of silicon steel sheets, IEEE Trans. Magn. 56 (3) (2020) 7512004.
[13] Y. Dou, Y. Li, Z. Lin, et al., An improved cross-yoke SST for accurate 1-D and 2-D magnetic testing of Fe-Si sheets, IEEE Trans. Instrum. Meas. 71 (2022) 1–10.
[14] Y. Maeda, S. Urata, H. Nakai, et al., Development of the apparatus for measuring magnetic properties of electrical steel sheets in arbitrary directions under compressive stress normal to their surface, AIP Adv. 7 (5) (2017) 056664.
[15] K.I. Yamamoto, S. Yanase, Effects of compressive stress normal to the surface of non-oriented electrical steel sheets, Int. J. Appl. Electromagn. Mech. 44 (3–4) (2014) 271–278.
[16] N. Alatawneh, T. Rahman, D.A. Lowther, et al., Design and analysis of a toroidal tester for the measurement of core losses under axial compressive stress, J. Magn. Magn. Mater. 432 (2017) 519–526.
[17] Takahiro, Mizuta, Yoshihiro, et al., Magnetic property of amorphous magnetic thin ribbon and its laminated bulk under tensile and compressive stresses, IEEE Trans. Magn. 54 (11) (2018) 1–5.
[18] J. Salach, Stresses influence on magnetic characteristics of amorphous ring cores for current transducers, J. Electrical Eng.-Elektrotechnicky Casopis 66 (7) (2015) 41–44.
[19] C. Zhang, Y. Li, J. Li, et al., Measurement of three-dimensional magnetic properties with feedback control and harmonic compensation, IEEE Trans. Ind. Electron. 64 (3) (2016) 2476–2485.
[20] P. Zhang, L. Li, Vibration and noise characteristics of high-frequency amorphous transformer under sinusoidal and non-sinusoidal voltage excitation, Int. J. Electr. Power Energy Syst. 123 (2020) 106298.
[21] S. Zhang, D. Chen, B. Bai, Study of a high-power medium frequency transformer using amorphous magnetic material, Symmetry 14 (10) (2022) 2129.
[22] N. Xia, M. Chen, X. Mao, et al., Laminated nanocrystalline-ferrite high saturation magnetic flux density composite core for use in high-frequency transformers, J. Power Electron. (2024) 1–11.
[23] B. Chen, X. Liang, N. Wan, Design methodology for inductor-integrated litz-wired high-power medium-frequency transformer with the nanocrystalline core material for isolated DC-link stage of solid-state transformer, IEEE Trans. Power Electron. 35 (11) (2020) 11557–11573.
[24] K. Yamamoto, T. Hamada, S. Yanase, Effects of compressive stress normal to the surface of grain-oriented electrical steel sheets, Int. J. Appl. Electromagn. Mech. 48 (2–3) (2015) 153–158.
[25] H. Helbling, A. Benabou, A. Van Gorp, et al., Effect on magnetic properties of inhomogeneous compressive stress in thickness direction of an electrical steel stack, J. Magn. Magn. Mater. 500 (2020) 166353.
[26] S. Huang, C.S. Ragusa, W. Xu, et al., Measurement of the vector magnetic property of electrical steel sheet under triaxial stress, IEEE Trans. Instrum. Meas. 73 (2024) 1–13.
[27] G. Herzer, Soft magnetic materials—Nanocrystalline alloys. Handbook of magnetism and advanced magnetic materials, 2007.
[28] V. Permiakov, L. Dupré, A. Pulnikov, et al., Loss separation and parameters for hysteresis modelling under compressive and tensile stresses, J. Magn. Magn. Mater. 272 (2004) E553–E554.